

An Innovative Polariscopes for Photoelastic Stress Analysis

Jon R. Lesniak¹, Michael J. Zickel¹, Christopher S. Welch², Deonna F. Johnson²

Abstract

An innovative polariscopes involving a single rotating optical element and a digital camera for full-field image acquisition allows automated data to be acquired quickly and efficiently. Software analysis presents the data in an easy to interpret image format depicting the magnitude of the shear strains and the directions of the principal strains.

Introduction

Photoelastic stress analysis has long been a faithful and productive technology offering the measurement community one of the earliest forms of full-field stress analysis. Unfortunately, its maturity has led to the misconception that the technology is no longer fertile ground for interesting developments, and consequently, photoelastic stress analysis is often overlooked by younger scientists. Several new automated polariscopes systems aimed at improving the efficiency and accuracy of photoelastic stress analysis have been introduced over the past several years [1, 2, 3, 4, 5]; however, each of these systems involves one or more complicated procedures such as fringe counting or phase stepping [6, 7] often making the polariscopes hard to use and the results difficult to interpret and not very intuitive. It is certainly true that many talented scientists have invented numerous photoelastic techniques, establishing many as fundamental concepts, but there are still many fields to plow. The importance of shear based failure criterion persists as does the need to validate numerical models with experimental techniques. Photoelastic stress analysis is a powerful analysis tool especially when combined with thermoelastic stress analysis. The combination makes available full-field stress tensor data. For photoelasticity to thrive it needs to keep pace with the turn key era. At the same time, it is important that advances in the technology do not exclude other recent improvements to the technology; therefore, a fully automated polariscopes with immediate and easily interpreted results, and the versatility to be integrated into current research is paramount. Furthermore, a simple and easily understandable description of the mechanics of the polariscopes is essential. One must feel comfortable with the measurement being made without requiring extensive study. By combining a rotating analyzer and a video lock-in system an

automated grey-field polariscopes has been devised that painlessly collects both magnitude and direction data without user intervention. Although the new polariscopes is capable of making multiple fringe measurements, it has its greatest impact in sub-fringe applications where the output parallels the description of the stress state of an object given by Mohr's circle.

Grey-field Polariscopes

Figure 1 is a simplified portrayal of the grey-field polariscopes. The object is illuminated with circularly polarized light. Upon propagation through a birefringent medium, or strained photoelastic coating, the light exits elliptically polarized. The resulting elliptical light is analyzed by an automatic ellipsometer in the form of a rotating analyzer, and the resulting light oscillations are analyzed by a video lock-in system.

In order to better describe the science behind the grey-field polariscopes each of the critical steps in the evolution of the light signal is broken out and explained through the following figures and mathematical discussion. The circularly polarized light entering the model (Fig. 2) is separated into two components, one component (A_1) parallel to the fast axes and another component (A_2) parallel to the slow axes. The fast axis makes an angle β with respect to a reference direction, in this case the horizontal axes. The circularly polarized light components are described by

$$A_1 = \frac{a}{\sqrt{2}} \cos(\eta t) \quad A_2 = \frac{a}{\sqrt{2}} \sin(\eta t) \quad (1)$$

After propagating through the coating whether in transmission or reflection, the slow axes can be modeled to have a phase lag Δ with respect to the fast axes. The overall retardation experienced by both paths is ignored for simplicity. The light exiting the coating now takes the form

$$A_1 = \frac{a}{\sqrt{2}} \cos\left(\eta t + \frac{\Delta}{2}\right) \quad (2a)$$

$$A_2 = \frac{a}{\sqrt{2}} \sin\left(\eta t - \frac{\Delta}{2}\right) \quad (2b)$$

where

¹ Stress Photonics Inc., 3002 Progress Rd., Madison, WI 53716

² College of William and Mary, Applied Science, Williamsburg, VA 23186

$$\Delta = \frac{4\pi hk}{\lambda} (\epsilon_1 - \epsilon_2) = f(\epsilon_1 - \epsilon_2) \quad (3)$$

where

k is the relative strain optic coefficient
h is the thickness,
 λ is the wavelength of light
f is the fringe value of the coating [8]

The light of Eqs. 2(a,b) is described as elliptically polarized, which is apparent when Eqs. 2(a,b) are rewritten as

$$A_{maj} = a \cos\left(\frac{\pi}{4} - \frac{\Delta}{2}\right) \cos\left(\eta t + \frac{\pi}{4}\right) \quad (4a)$$

$$A_{min} = a \cos\left(\frac{\pi}{4} + \frac{\Delta}{2}\right) \sin\left(\eta t + \frac{\pi}{4}\right) \quad (4b)$$

The major axis of the ellipse is always shifted $\pi/4$ radians from the direction of the first principal strain for odd fringes and $-\pi/4$ for even fringes (Fig. 3). If an analyzer is placed in the system at an orientation α (Fig. 4) from the major axis the resulting light amplitude is described by

$$A_\alpha = \cos\alpha A_{maj} + \sin\alpha A_{min} \quad (5)$$

The intensity of the resulting light is related to the square of the amplitude which after several trigonometric manipulations yields

$$I = A_\alpha^2 = \frac{a^2}{2} [1 + \cos(2\alpha) \sin \Delta] \quad (6)$$

The peanut shape of the light intensity results from squaring the elliptical light. If the analyzer is allowed to rotate at an angular frequency ω then

$$\alpha = \omega t - \beta - \frac{\pi}{4} \quad (7)$$

It is assumed that the analyzer is parallel with the reference orientation at $t=0$. In terms of time, the intensity map is described by

$$I = \frac{a^2}{2} [1 + \sin 2(\omega t - \beta) \sin \Delta] \quad (8)$$

From this relation it can be seen that in the absence of birefringence the output is a neutral grey. It can also be seen that in the presence of birefringence the amplitude of the signal oscillates about this neutral grey level. The oscillating portion of the signal is zero when the axis of analyzer coincides with the principal strain axes. It should also be noted that only the amplitude measurement is affected by the color of the input light. The orientation of the major axis is unaffected.

Sub-fringe PSA

Sub-fringe PSA assumes small retardation angles so that the amplitude of the oscillations can be directly related to the amplitude of the shear strains. For very small retardation angles Eq. 8 can be rewritten as

$$I = \frac{a^2}{2} [1 + \Delta \sin 2(\omega t - \beta)] \quad (9)$$

For larger angles some linearization may be required.

Video Lock-in

In order to make extremely accurate measurements of sub-fringe birefringence a video lock-in algorithm is employed. The analyzer and an absolute position encoder are rotated at a constant angular velocity and the computer monitors the readout of the encoder (Fig 5). When a prescribed angle is crossed an image is captured and stored for subsequent processing. In this study eight images are captured for every one half revolution of the analyzer. The angles at which the computer triggers the capture of an image are defined by

$$\theta_n = \frac{\pi(n-1)}{N} \Big|_{n=1}^N \quad (10)$$

It is important to recall that a full period of signal oscillation is represented by one half of an analyzer revolution.

By controlling the image sampling in this manner a level of synchronization is achieved and the lock-in algorithm that is performed takes the simple form described by

$$X(x, y) = \frac{2}{N} \sum_{n=1}^N J_n(x, y) \sin(2\pi n / N) \quad (11a)$$

$$Y(x, y) = \frac{2}{N} \sum_{n=1}^N J_n(x, y) \cos(2\pi n / N) \quad (11b)$$

where J_n is a sampled image.

From Eqs. 11(a,b) the amplitude and direction of shear strains can be determined by the following relations

$$\gamma = K \sqrt{X^2 + Y^2} \quad (12)$$

where K is a calibration constant including system gains, light intensity variations and residual strains in the coating. The phase is calculated from the X and Y images as

$$\phi = \text{Tan}^{-1}\left(\frac{Y}{X}\right) \quad (13)$$

The orientation of the first principal strain direction to the reference direction (β) is related to ϕ by

$$\phi = 2\beta \quad (14)$$

For odd fringes β points in the direction of the first principal strain, and for even fringes β points in the direction of the second principal strain.

The results of Eqs. 12–14 are identical to the equations describing Mohr's circle (Fig 6) where X is the base, Y is the height and the angle β represents the physical angle on the specimen. This means that the results of this polariscope directly yield in-plane shear strain components for any arbitrary direction. Also, this implies that in the linearized area, the XY image sets can be operated on as vectors. The superposition of two strain states can be calculated by adding two XY image pairs then applying Eqs. 12 and 13 to find magnitude and direction. To remove the effects of residual strain in the coating an initial XY pair can be captured and subtracted from the images collected after loading. The magnitude and direction are then calculated after the subtraction.

Experimental Setup

As seen in Fig. 5, a simple yet flexible optical setup was used. The light source consists of a standard light bulb which projects white light through a condenser lens, a filter (optional), a polarizer and, finally, a quarter waveplate. Circularly polarized light is projected onto the area of interest. The polariscope is positioned at a shallow angle with respect to the light source. Within the projector, a relay lens projects a virtual image of the small video detector into free space. This creates physical space to incorporate the rotating analyzer and other calibration devices. The rotating analyzer is positioned near the image plane of the virtual detector in order to eliminate jitter effects caused by the refractive variations in the polarizer sheet. A field lens condenses the optical path so that a standard camera lens with a c-mount adapter can be used. The position of the analyzer is monitored by the absolute position encoder. The computer monitors the status of this encoder and triggers the frame-grabber at predetermined angles. As mentioned above the use of predetermined angles allows the use of a simple lock-in algorithm. The sampled images are processed by the computer and displayed in both magnitude and direction.

Results

A beam in four-point bending was used as the test specimen. The beam (3.175 mm thick aluminum) was coated with a commercially available photoelastic sheet coating (0.254 mm thick) and loaded at approximately 1kN. The stress state of the beam is depicted in the schematic of figure 7. The shaded areas illustrate one of the key advancements introduced with the grey-field polariscope. With a standard circular or plane polariscope it is not possible to distinguish between tension and compression, but the grey-field polariscope uses what can be thought of as an offset to add sign to tensile and compressive stress making the two distinguishable.

Results using the polariscope are shown in Figs. 8 and 9. The horizontal or x-axis was chosen as the reference axis, so that, for this example, the Y, or cosine, image is zero. The signal to noise ratio was improved by collecting data over four oscillations of the analyzer, so that each X and Y image is a sum of eight images ($J_1 - J_8$). The magnitude and phase images in Fig. 9a and 9b are calculated according to Eqs 12 and 13. The magnitude image has the characteristic neutral axis down the center of the sample. Direction lines are superimposed on the direction data according to the calculated pixel values in the image, and they clearly indicate a horizontal (0°) and vertical (90°) orientation on either side of the neutral axis, just as one might anticipate.

Operational Modes

There are many procedural options that can improve the collected data. Several goals leading to the improvement are:

- Determine system gain
- Compensate for illumination variations
- Compensate for coating residual strains
- Compensate for quality of projected light

There are several methods that might accomplish these goals. The following outlines one experimental procedure that can eliminate all of the afore mentioned concerns.

Polarization Quality

For typical operation, monochromatic light is used and the quality of the circular polarization is quite good, eliminating any need for compensation. In other applications, polychromatic light may be desired, and in these cases, perfect circular polarization may not be achievable. A correction for this problem may be made by placing a diffuse reflective target in the field-of-view, and performing the video lock-in procedure. The analysis will yield the degree of imperfection in the polarized light, thus providing a means of compensation. Essentially, the imperfection will be a constant full-field offset that is easily determined. In the case of polychromatic light an offset for each color must be acquired.

Light Intensity and System Gain

Light intensity variations and pixel by pixel system gains can be determined separately or together. The following is a simple approach to calibrate the above mentioned parameters and to establish the correct phase of the lock-in, which effectively sets the reference orientation. To accomplish all of the above in the sub-fringe mode a calibration plate of birefringence δ can be introduced into the system to augment the existing birefringence. This apparent strain can be resolved by subtraction of the loaded image from the loaded-augmented

image. From this information light intensity can be calculated free of reflection error.

An alternative to this approach is to use the average of the images as the intensity and to calibrate the system gains separately. This approach will be more important as the speed of grey-field polariscope systems increases and dynamic strains are monitored.

Residual Strains and Load Ramping

Residual strains can be eliminated simply by load differencing. Essentially an image is run through the paces as described above then the load is increased and the process is repeated. The difference between these images will compensate for residual strains and/or light source imperfections.

Load ramping is also useful for imaging large or complex components that exhibit a wide range of strain values. With this technique a low load is initially used so that regions exhibiting high strain fields can be interrogated with good resolution and without exceeding sub-fringe limitations. The load is then increased so that regions with lower strain values can be sampled with optimal resolution. By using the load ramping technique all regions on the sample can be inspected with optimal resolution. The extent of the dynamic range of the response defines the number of loads that should be used. This method can significantly increase the apparent dynamic range.

Conclusion

A fully automated polariscope system that determines the magnitude and direction of the shear strains has been developed. This grey-field polariscope also automatically distinguishes between the directions of the principal strains, and indicates each direction in the resultant data. The data are presented in an intuitive format so that they are easy to interpret. One image depicts the shear strain magnitude with gradients represented in greyscale levels, and the other indicates the directions of the principal strains. Interpretation of the data parallels the strain state description given by Mohr's circle.

The grey-field polariscope utilizes a video lock-in algorithm to achieve a high degree of sensitivity, which makes it ideal for subfringe operation. This does not exclude higher order fringe

operation, where techniques such as load ramping can be used to great advantage.

Acknowledgments

The authors would like to acknowledge NASA Langley Research Center and in particular Mr. K. Elliott Cramer for supporting this research through the STTR (Small Business Technology Transfer) program. In addition, Mr. Ted Tuttle of Stress Photonics Inc. contributed extensively in the design and construction of the polariscope and light source.

References

- [1] Patterson, E. A., Wang, Z. F., "Towards Full-field Automated Photoelastic Analysis of Complex Components," *Strain*, May, 49-56, 1991.
- [2] Redner, S., "New Automatic Polariscope System," *Experimental Mechanics*, December, 486-491, 1974.
- [3] Redner, S., "Compensation Method Using Synchronized Polarizer-Analyzer Rotation," *Experimental Mechanics*, June, 221-224, 1976.
- [4] Robert, A. J., "New Methods in Photoelasticity," *Experimental Mechanics*, May, 224-232, 1967.
- [5] Voloshin, A. S., Burger, C. P., "Half-fringe Photoelasticity: A New Approach to Whole-field Stress Analysis," *Experimental Mechanics*, September, 304-313, 1983.
- [6] Hecker, F. W., Morche, B., "Computer Aided Measurement of Relative Retardation in Plane Photoelasticity," *Proceedings of the VIIIth International Conference on Experimental Stress Analysis*, May, 535-542, 1986.
- [7] Asundi, A., "Phase Shifting in Photoelasticity," *Experimental Techniques*, January/February, 19-23, 1993.
- [8] Measurements Group Tech Note, TN-701, Measurements Group, Inc., P.O. Box 27777, Raleigh, NC, 1977.

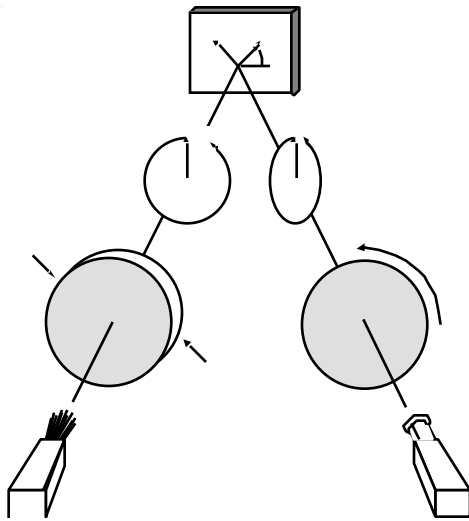


Figure 1. Grey-field reflection polariscope

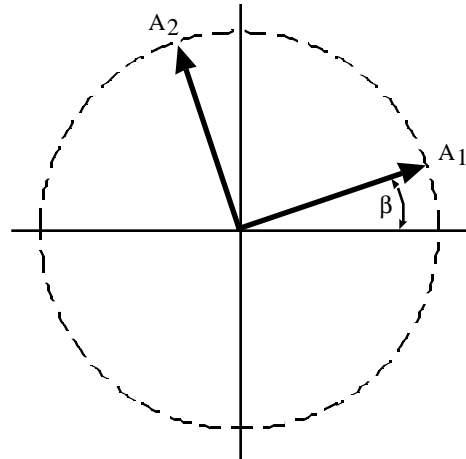


Figure 2. Circularly polarized light

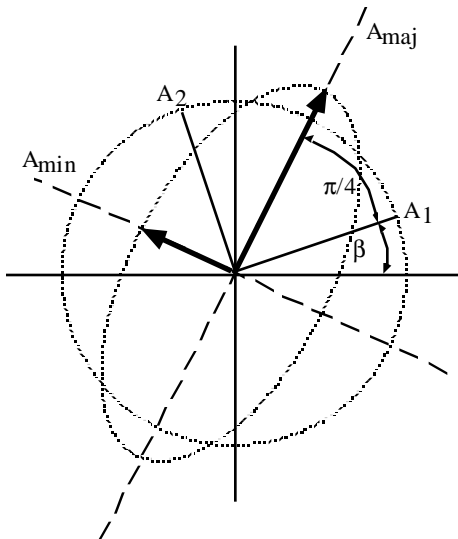


Figure 3. Elliptically polarized light

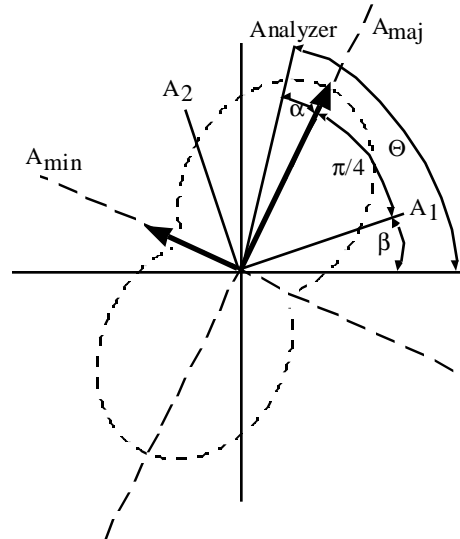


Figure 4. Light intensity resulting from squaring the amplitude of the elliptically polarized light

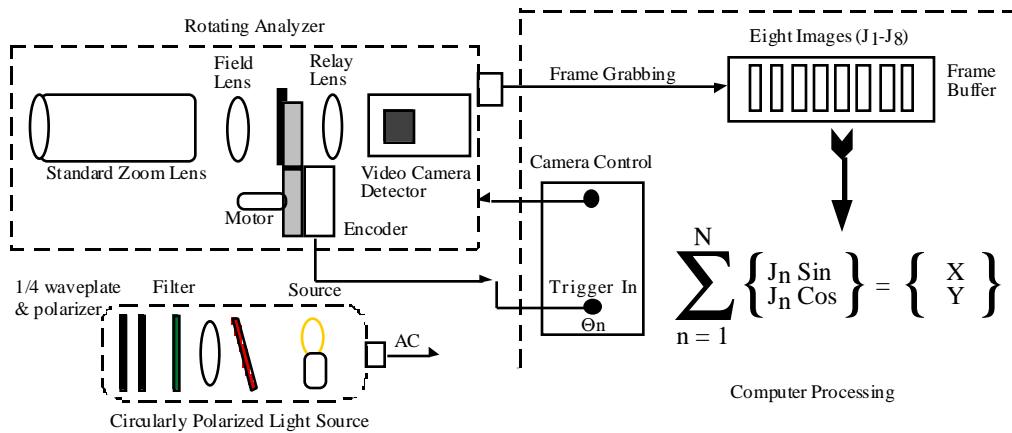


Figure 5. Experimental system

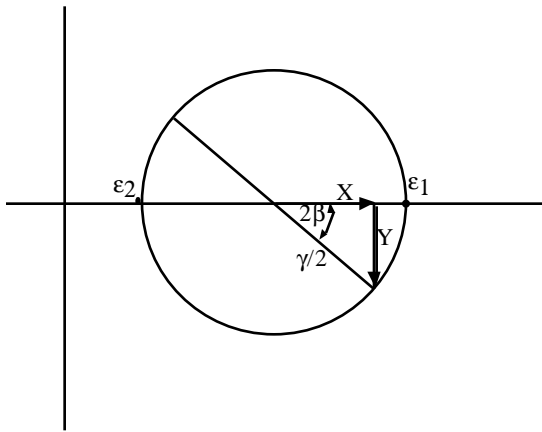


Figure 6. Mohr's circle

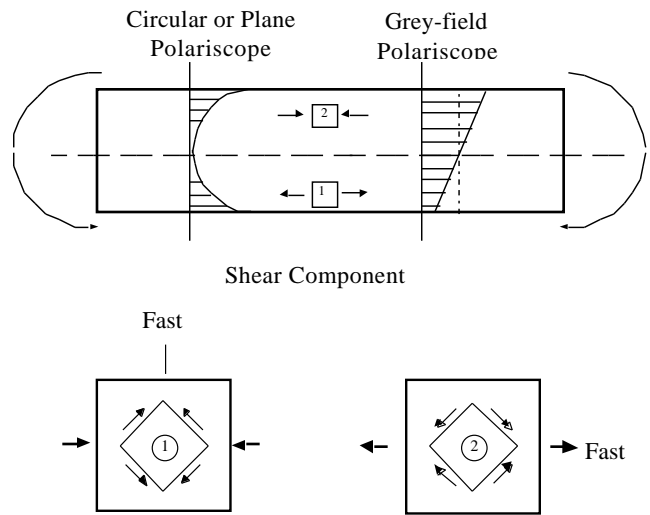


Figure 7. Schematic of beam in bending

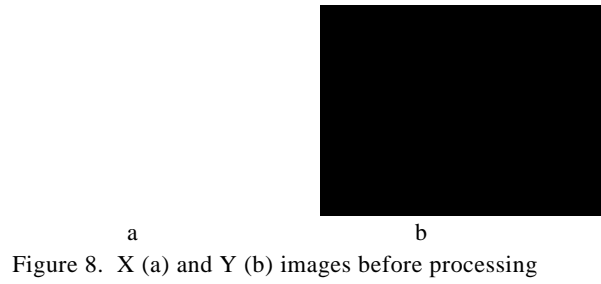


Figure 8. X (a) and Y (b) images before processing

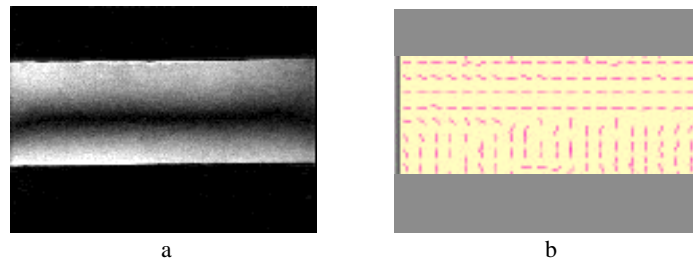


Figure 9. Images showing the magnitude (a) and the direction (b) of the principal strains